PAPER

Failure criterion for graphene in biaxial loading—a molecular dynamics study

To cite this article: Hessam Yazdani and Kianoosh Hatami 2015 *Modelling Simul. Mater. Sci. Eng.* **23** 065004

IOP Publishing Modelling and Simulation in Materials Science and Engineering

Modelling Simul. Mater. Sci. Eng. **23** (2015) 065004 (14pp) doi:10.1088/0965-0393/23/6/065004

Failure criterion for graphene in biaxial loading—a molecular dynamics study

Hessam Yazdani and Kianoosh Hatami

School of Civil Engineering and Environmental Science, The University of Oklahoma, 202 W Boyd St, Room 450B, Norman, OK 73019, USA

E-mail: yazdani@ou.edu and kianoosh@ou.edu

Received 2 December 2014, revised 19 May 2015
Accepted for publication 22 June 2015
Published 17 July 2015

Abstract

Molecular dynamics simulations are carried out in order to develop a failure criterion for infinite/bulk graphene in biaxial tension. Stresses along the principal edge configurations of graphene (i.e. armchair and zigzag directions) are normalized to the corresponding uniaxial ultimate strength values. The combinations of normalized stresses resulting in the failure of graphene are used to define failure envelopes (limiting stress ratio surfaces). Results indicate that a bilinear failure envelope can be used to represent the tensile strength of graphene in biaxial loading at different temperatures with reasonable accuracy. A circular failure envelope is also introduced for practical applications. Both failure envelopes define temperature-independent upper limits for the feasible combinations of normalized stresses for a graphene sheet in biaxial loading. Predicted failure modes of graphene under biaxial loading are also shown and discussed.

Keywords: graphene, biaxial tension, hyperelastic materials, molecular dynamics, failure envelopes

(Some figures may appear in colour only in the online journal)

1. Introduction

Graphene is a monatomic thick sheet of sp^2-hybridized carbon. Its extended hexagonal lattice is the motif of carbon allotropes (i.e. graphite (3D), nanotubes (1D) and fullerenes (0D) [1]). Since its discovery [2] (or more accurately, isolation), graphene has allured academic and industrial interest owing to its exceptional electronic [3], optical [4], thermal [5] and mechanical properties. As a lightweight material but the strongest and stiffest ever known in the universe [6], graphene holds promise as a reinforcing agent for composite materials [7]. In addition, the unique attribute of graphene in generating enormous strain-induced pseudo-magnetic fields opens the door for its application in nanoelectromechanical systems [8, 9].

The exceptional mechanical properties of graphene have been consistently corroborated via first-principles (i.e. *ab initio*) calculations, semiempirical methods, laboratory experiments and numerical simulations. By means of first-principles calculations, Konstantinova *et al* [10] reported a Young's modulus of 1.24 ± 0.01 TPa for graphene. Using the density functional perturbation theory, Liu *et al* [11] calculated the graphene's Young's modulus and Poisson's ratio as 1.05 TPa and 0.186, respectively. The strengths of 121 and 110 GPa in the zigzag (ZZ) and armchair (AC) directions, respectively, were also reported for graphene [11]. In addition, by nanoindenting the center of a free-standing graphene membrane in an atomic force microscope, Lee *et al* [12] measured the strength and Young's modulus of graphene to be 130 ± 10 GPa and 1 TPa, respectively (the corresponding values for the structural steel are 0.36 GPa and 0.21 TPa, respectively).

Due to its exceedingly small dimensions, it is challenging to pinpoint the properties of graphene via laboratory experiments. First-principles calculations are also computationally intensive. Alternatively, experimentally validated molecular dynamics (MD) simulations have provided researchers with a virtual laboratory to probe the what-if scenarios that would otherwise be difficult (if not impossible) to investigate in the laboratory. MD simulations have shown that graphene exhibits an orthotropic behavior with different ultimate strength values along the zigzag and armchair directions [13]. MD simulations have also demonstrated that the mechanical response of graphene nanoribbons (GNRs) is nonlinear elastic and their size and chirality have significant influences on their mechanical properties [13]. It has been reported that 8 nm constitutes a critical width for GNRs beyond which the size effect largely disappears and their elastic properties converge to the values for bulk/infinite graphene [13, 14]. In addition, MD simulations have shown that while the Young's modulus of graphene remains fairly insensitive to the temperature up to 1200 K, the values of its failure strength and strain undergo a steady fall as temperature is increased from the absolute zero [15, 16].

In spite of a fairly considerable number of MD studies on the mechanical properties of graphene, to the best of the authors' knowledge, the behavior of graphene in biaxial loading has been the subject of only a few analytical studies. Marianetti and Yevick [17] used the density functional theory to investigate the failure mechanism of graphene under a generic state of tension (including biaxial tension) at absolute zero temperature. They concluded that the uniaxial failure of graphene is caused by elastic instability while graphene maintains its symmetrical structure. However, a soft-mode phonon instability, where the phonon frequency for some wavevectors vanishes, promotes failure in graphene when subjected to equi-biaxial tension. These findings are merely applicable to low temperatures where all atomic motions in a crystal can be decomposed into phonon-independent modes [11]. Volokh [18] and Tuleubekov *et al* [19] used a combination of continuum and molecular mechanics to study the behavior of graphene in biaxial loading. In both of the latter studies, graphene was decomposed into two simple Bravais lattices in order to tailor it to the continuum mechanics framework. None of the studies mentioned above reported a closed-form failure criterion for graphene. Furthermore, due to the limitations of the methods employed (i.e. continuum and molecular mechanics), the influence of temperature on the biaxial strength of graphene was not considered.

This paper reports a series of MD simulations which were carried out on defect-free infinite graphene models in order to develop a simple failure criterion for graphene in biaxial loading. Whether failure criteria should be expressed in terms of stress or strain has been a longstanding issue dating back to the emergence of the theory of materials failure. Although discussions on the subject remain inconclusive, it is supposed that characterizing failure criteria in terms of stress is more compatible with the physics of failure (e.g. dislocation dynamics in the ductile range) [20]. In this paper, and in the supporting studies upon which it is based, stress is taken as the fundamental form to express the failure of graphene. In this regard, the simulation

cases investigated in this paper were different from one another with respect to the applied transverse stress magnitudes. The influences of temperature and strain rate were also studied. The findings of this study can help to improve the design, reliability and functionality of the nanoscale devices made from graphene and provide a fairly simple computational tool to study the mechanical response of graphene to tensile loading. Investigation on the detrimental impacts of defects and imperfections in graphene on its performance and failure in biaxial loading is reserved for a future study.

2. Molecular dynamics simulations

All the simulations in this study were carried out using the MD package LAMMPS [21]. Details of the simulations are described in the following sections.

2.1. Simulation models

Simulations were carried out on a 82.95 Å × 82.28 Å (zigzag × armchair) monolayer graphene sheet consisting of 2720 carbon (C) atoms with an equilibrium bond length of 1.42 Å and a bond angle of 120°. The sheet was considered adequately large (width > 80 Å [14]) to avoid the finite-size effects and to represent infinite graphene. Periodic boundary conditions were applied at all four edges in order to simulate the infinite dimensions of the sheet, further minimize the size effects, eliminate the effects of free edges on the mechanical properties of graphene and finally, guarantee constant strain in the desired loading direction.

2.2. Interatomic potential

The adaptive intermolecular reactive empirical bond-order (AIREBO [22]) potential and the corresponding parameters were used to define the interactions between carbon atoms in graphene. The AIREBO potential has been shown to accurately capture the bond interaction, bond rupture and bond reformation between carbon and hydrogen atoms in the MD studies on carbonaceous and hydrocarbon systems [13, 23]. In the original version of the potential, a three-step function was proposed to specify the interaction between nearest-neighbor carbon atoms. In this function, two bonded carbon atoms fully interact with one another as long as their bond length is below 1.7 Å. When the C–C bond length exceeds 1.7 Å, a cutoff function is actuated in order to attenuate the interaction between the adjacent carbon atoms until the bond length reaches 2.0 Å, where the interaction is terminated and the bond ruptures. The three-step cutoff function, however, generates spurious bond forces near the cutoff distance, especially at low temperatures, due to a discontinuity in its second derivative [14]. Consequently, graphene exhibits a non-physical strain hardening behavior at a C–C bond length of 2.0 Å [24, 25]. In this study, as proposed by several researchers (e.g. [24]), the intermediate step of the function (1.7 Å < bond length < 2.0 Å) was omitted by setting both its lower and upper limits to 2.0 Å. This ad hoc approach solved the aforementioned cutoff problem while it preserved the ability to describe bond breaking and the nearest-neighbor character of interactions.

It should be noted that the cutoff function in the AIREBO potential is restricted to bond breaking and rehybridization and cannot be used to quantify bond reformation in carbonaceous materials. However, ruptured bonds are generally unlikely to reform in fractured graphene unless the stress that causes a bond to stretch is significantly reduced or completely removed. In this case, other potentials (e.g. spontaneous thermal fluctuations) could bring a pair of atoms that are connected by a bond closer to each other than their breaking distance

and thereby reform their bond [26]. In addition, the studies on defective graphene have consistently shown that its ultimate strength is proportionally lower as a function of the defect coverage up to approximately 7–10% and levels off to the strength of a highly defective graphene for more extensive defects [27]. Therefore, it is expected that randomly distributed bond reformations (if any) will not considerably change the ultimate strength of graphene. However, bond reformation might significantly increase the magnitude of strain at failure and, consequently, improve the ductility of graphene, giving another justification for expressing the failure criterion in terms of stress in this study.

2.3. Calculation of stresses and strains

A great number of approaches have thus far been proposed to define the stress tensor in atomistic mechanics, and many relationships have been developed to bridge the atomistic stresses to the macroscopic quantities in continua. In this study, the virial stress (also known as local atomic level stress or total stress) was used to calculate the atomistic stresses due to its simple form and ease of calculations. By definition, each virial stress component per unit volume within the graphene sheet is the aggregate of the corresponding stresses over all carbon atoms (each denoted by α) in the sheet and is calculated as [28, 29]:

$$\sigma_{ij} = \frac{1}{\Omega}\sum_{\alpha}\left(\frac{1}{2}\sum_{\beta=1}^{N} r_i^{\alpha\beta} f_j^{\alpha\beta} - m^{\alpha} v_i^{\alpha} v_j^{\alpha}\right), \tag{1}$$

where i and j (which can take x, y and z) denote direction of the normal to the stress plane and the corresponding traction applied, respectively; β is an atom index running from 1 to N; N is the number of neighboring atoms for atom α; $r_i^{\alpha\beta}$ is the distance between atoms α and β along the ith direction; $f_j^{\alpha\beta}$ is the force along the jth direction on atom α due to atom β; m^{α} is the mass of atom α; v_i^{α} and v_j^{α} are the components of the thermal excitation velocity of atom α; Ω is the total volume of graphene, assuming a thickness of 3.35 Å.

It should be noted that the first term on the right-hand side of equation (1), known as the potential term, takes into account the interatomic forces acting on an arbitrary plane, while the second, known as the kinetic term, considers the momentum flux intercepted by it [28]. Whether or not including the kinetic term in the virial expression yields atomistic stresses analogous to those measured by the Cauchy expression on a continuum scale has been a contentious topic in the literature. Premising on the fact that the stress in the Cauchy definition is stated solely in terms of the internal mechanical forces between different points in a body, Zhou [30] asserted that the contribution of the kinetic term to the stress tensor is at odds with the Cauchy definition and provided some examples to demonstrate that the two expressions are not equivalent. Some researchers adopted this notion and tried to derive new atomistic stress definitions equivalent to the Cauchy stress (e.g. see [31]). However, for a material such as graphene, the application of the continuum mechanics principles to measure its stresses typically leads to a residual stress at zero strain, particularly at elevated temperatures, which can be eliminated by using the virial stress (i.e. excluding the contribution of kinetic energy) [16]. The interested reader is referred to [25] for further details.

For practical applications, the engineering (nominal) strain, defined as the elongation relative to the original length, was used to calculate the elastic properties of graphene and to plot its stress–strain response [32]. The ultimate stress (σ_u) and strain (ε_u) values used in the analysis correspond to the point at the peak of the stress–strain plot.

2.4. Simulation sequence

In the simulations that were carried out in this study, the initial structure of each infinite graphene model was subjected to an equilibration sequence as described below to relax any high energy configurations. A time step of 0.5 fs (0.5×10^{-15} s) was used in all simulations, in accordance with related previous studies (e.g. [33]). Five temperatures of 1, 300, 500, 1000 and 1500 K were examined. For each temperature, the simulation initially ran for 40 ps (80 000 time steps) using NPT (isothermal–isobaric) ensemble at a temperature 200 K greater than the desired temperature and zero pressure components along the in-plane directions followed by relaxation for 30 ps at that temperature. The Nosé–Hoover thermostat and barostat were employed to control temperature and pressure, respectively. The subsequent relaxation cooled the structure down to the desired temperature over a period of 40 ps maintaining the pressure components at zero. Eventually, the structure was further relaxed for 30 ps at the desired temperature. The potential energy history of the sheet was observed to ensure negligible energy drift at the end of each stage. In addition, the microstructure of the sheet was frequently visualized in order to ensure that it was appropriate for deformation simulations.

Three loading régimes which were different in their sequence of loading along the zigzag and armchair directions were used to investigate the behavior of graphene in biaxial tension. In régime I, the boundaries of the sheet were first decoupled from the NPT equations of motion [34]. Subsequently, the sheet was elongated at a constant strain rate using NVT (canonical) ensemble along the zigzag direction until a certain level of stress along that direction was mobilized. Next, the strain along the zigzag direction was held constant and the sheet was stretched along its armchair direction until failure. The second régime (régime II) was used in order to test the hypothesis that reversing the sequence of the transverse loadings from zigzag–armchair to armchair–zigzag would not significantly change the combination of stresses resulting in failure. In this régime, the sheet was first stretched along the armchair direction and then elongated to failure along the zigzag direction. Régime III included equi-biaxial loading, where the sheet was simultaneously stretched along both directions until failure.

A strain rate of 0.001 ps was used for all the loading régimes used in this study. Strain rates of this order are very common in MD simulations (e.g. see [16, 35]). The experimental strain rates, in contrast, are on the order of $1\,\mathrm{ms}^{-1}$ [12, 36]. MD simulations at low strain rates are computationally prohibitive for the studies described in this paper, where a great number of simulations would be required to obtain meaningful results. The database generated in the present study is the result of 330 simulations with different combinations of temperature, loading régime and stress magnitudes within the first loading stage for régimes I and II. Considering the fact that each simulation in this study took on average 8 min on a supercomputer to complete, selecting a lower strain rate would have exponentially increased the required computational demand and time, making the study very lengthy, if not impossible. Nevertheless, régime III (i.e. equi-biaxial loading) was repeated for two additional strain rates of 10^{-5} and $0.1\,\mathrm{ps}^{-1}$ in order to investigate the strain rate-dependent failure properties of graphene in biaxial loading, and it was assumed that the results would hold for the other loading régimes.

3. Results and discussions

The influence of temperature on the ultimate strength of graphene is shown in figure 1. The results indicate that the mechanical performance of graphene is temperature-dependent and anisotropic (orthotropic) in that its ultimate strength varies in the AC and ZZ directions and deteriorates with temperature. In an independent separate simulation, it was observed that the graphene sheet completely restored its original configuration after a loading–unloading cycle,

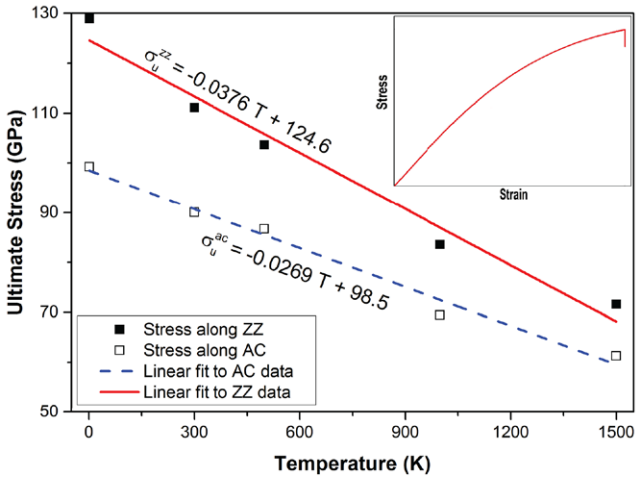

Figure 1. Variations of predicted ultimate strength of graphene in zigzag (ZZ) and armchair (AC) directions with temperature subjected to uniaxial loading (strain rate = 0.001 ps^{-1}). The inset shows a schematic nonlinear behavior expected for graphene based on MD simulations. The data points at each temperature represent the mean values over three independent numerical experiments.

which indicated that it was completely elastic even when unloaded from stresses approaching failure. This observation together with the typical nonlinear stress–strain response (inset of figure 1), which has been attributed to the anharmonic terms of the C–C interatomic potential [37], suggest that the mechanical response of graphene prior to failure is nonlinear elastic (hyperelastic).

Typical biaxial stress–strain responses of graphene as calculated in this study are shown in figure 2. According to figure 2(a), in the staged loading régimes (i.e. régimes I and II), when the sheet is stretched from its initial unloaded configuration along a primary direction (either zigzag or armchair), stress is developed in both the primary (σ_p^I) and transverse (σ_s^I) directions, albeit at different rates in order to maintain the equilibrium of the sheet.

During the second stage of loading (i.e. loading to failure), where the primary and secondary directions are interchanged, the stress along the secondary direction (previously the primary direction) initially increases as a result of continued elongation along the primary direction. Further elongation along the primary direction lowers the stress along the normal direction, possibly due to the reduction in the stiffness of the sheet as it approaches failure. Eventually, a combination of stresses along the two mutually orthogonal directions (σ_p^{II} and σ_s^{II}) leads to failure in the sheet. In Régime III (i.e. equi-biaxial loading), the stresses along the zigzag and armchair directions increase synchronously until they collectively result in failure in the graphene sheet (figure 2(b)).

In presenting the simulation results for failure envelopes of graphene in biaxial loading, the failure stress values calculated in each direction (i.e. ZZ and AC) were normalized with respect to the corresponding uniaxial ultimate strength values (σ_u^{zz} and σ_u^{ac}). Hence, the following stress ratios were defined along the zigzag and armchair directions to normalize the calculated failure stresses in each direction:

$$\gamma^{zz} = \frac{\Delta\sigma^{zz}}{\sigma_u^{zz}}, \tag{2}$$

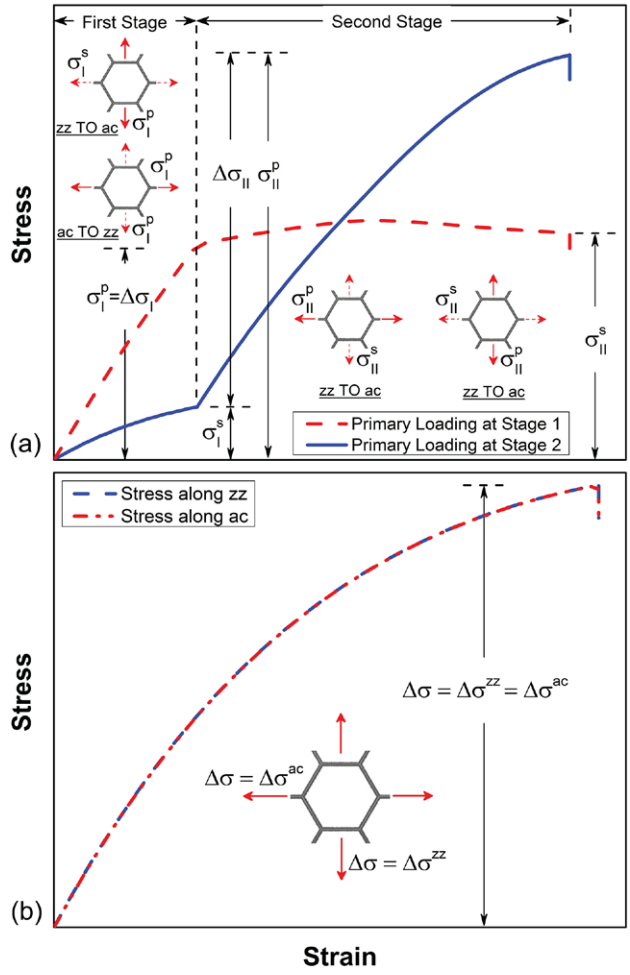

Figure 2. Typical stress–strain behavior of bulk graphene in (a) staged (régimes I and II) and (b) equi- (régime III) biaxial loading.

$$\gamma^{ac} = \frac{\Delta\sigma^{ac}}{\sigma_u^{ac}}, \tag{3}$$

where $\Delta\sigma^{zz}$ and $\Delta\sigma^{ac}$ are defined below for each loading régime (figure 2):

Régime I (zigzag–armchair):

$$\Delta\sigma^{zz} = \Delta\sigma_I; \quad \Delta\sigma^{ac} = \Delta\sigma_{II}, \tag{4}$$

régime II (armchair–zigzag):

$$\Delta\sigma^{zz} = \Delta\sigma_{II}; \quad \Delta\sigma^{ac} = \Delta\sigma_I, \tag{5}$$

régime III (equi-biaxial):

$$\Delta\sigma^{zz} = \Delta\sigma^{ac} = \Delta\sigma. \tag{6}$$

The MD simulation data corresponding to the failure of graphene at different temperatures and loading régimes in $\Delta\sigma^{ac}$–$\Delta\sigma^{zz}$ space are shown in figure 3. The notation $\Delta\sigma$ indicates

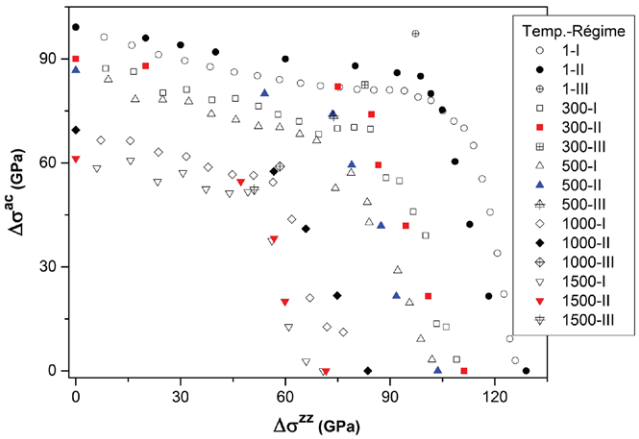

Figure 3. Combinations of biaxial stresses resulting in failure in graphene at different temperatures and loading régimes (strain rate = 0.001 ps^{-1})

incremental virial stress in graphene. Results indicate that the biaxial strength of graphene decreases at higher temperatures. Since both $\Delta\sigma^{ac}$ and $\Delta\sigma^{zz}$ approach the corresponding uniaxial ultimate strength values in the absence of the cross-direction loading as given in figure 1 (i.e. values at the *x*- and *y*-axes in figure 3), the biaxial strength of graphene decreases at higher temperatures at the same rate as its uniaxial strength in either direction. For instance, the area bound by the data points corresponding to a room temperature of 300 K in figure 3 is reduced by nearly 50% at an elevated temperature of 1000 K. Consistently stronger performance of graphene at lower temperatures is possibly due to the fact that low temperatures obstruct the nucleation of discrete local failures within the graphene structure, thus enabling it to withstand larger loads before failure [11, 38]. In addition, a greater C–C bond length at higher temperatures due to the thermal fluctuations arising from kinetic energy leads C–C bonds to store higher potential energy. Therefore, the initial configuration of the graphene sheet stores less strain energy at lower temperatures. According to the total strain energy theory (Beltrami–Haigh's theory), a body subjected to a combined stress state fails when the total strain energy exceeds the total strain energy corresponding to simple tension. Therefore, the graphene sheet at lower temperatures can accommodate larger stresses and strains before failure.

It can also be observed that for any given simulated temperature, the failure stress combinations corresponding to Loading régimes I and II (sequential biaxial loading) are comparable. However, those for the loading régime III (simultaneous biaxial loading) indicate a comparatively stronger response, especially at lower temperatures. This observation can be explained by the counteracting effects of the transverse forces on the changes in the bond angles of the sheet. The decrease in the bond angles due to the ZZ stress is partially neutralized by the tendency of the AC stress to widen the bond angles, thus minimizing the contribution of bond angles in the total strain energy of the sheet. As a result, the capacity of the sheet to store strain energy and, therefore, its strength increases.

Theoretical analyses and numerical simulations have identified two distinct modes of failure for defect-free graphene under a tensile load: brittle cleavage rupture and ductile failure by plastic flow instability. Brittle cleavage rupture, which prevails at low temperatures and high strain rates, is associated with sudden bond breaking and tearing along the fracture plane, leading to the formation of large open-ring structures. In contrast, external conditions such

as slow strain rates and high temperatures (greater than 1000 K [39] and below carbon's sublimation point: 3900 K [40]) favor dislocation-induced plastic flow, which is characterized by localized bond rotations at a crack tip [41]. At room temperature, defect-free graphene is intrinsically brittle, manifested by a catastrophic fracture observed in the nanoindentation of free-standing graphene membranes [12]. It is noteworthy that defective graphene (e.g. graphene with randomly distributed vacancies or Stone–Wales defects) exhibits ductility as a result of a complicated interplay among crack trap, crack-tip blunting and the structural rearrangement around the defects [27].

The failure modes of graphene under the three loading régimes at 0 K are shown in figure 4. For the Loading régime I (i.e. staged loading ZZ followed by AC), fracture nucleation occurs exclusively at some flaws along the armchair edges where the tensile stress exceeds the C–C bond strength (figure 4(a)). An infinitesimal additional strain (i.e. 18.17% versus 18.18%) results in the very fast formation and growth of cracks on the plane of maximum principal stress (i.e. ZZ direction), leading to brittle cleavage fracture. In contrast, in the loading régime II (i.e. staged loading AC followed by ZZ), cracks are initiated at a stochastic flaw at the interior lattice and grow at relative angles of 60° or 120°, indicating that failure is aligned with the crystallographic directions of graphene (figure 4(b)). Similar to régime I, fracture nucleation in régime III occurs at some flaws along the armchair edges (figure 4(c)). Cracks initially grow along the crystallographic directions of graphene, but are subsequently deviated due to the simultaneously and equally increasing stresses along the AC direction, resulting in the branching (splitting) and microscopic tortuosity of cracks. Similar failure modes were observed for graphene at room temperature in the numerical simulations carried out in this study. It is also noteworthy that the formation of suspended atomic chains immediately before failure (figures 4(b) and (c)) is consistent with laboratory observations [42] and first-principles calculations [43].

The influence of strain rate on the failure properties of graphene subjected to equi-biaxial loading is summarized in table 1. Results clearly show that both the stress and strain at failure increase with strain rate. However the influence of strain rate is significant only at higher temperatures (>~500 K) and is relatively insignificant compared with that due to temperature variations. These observations are consistent with those reported in [15, 16].

The data corresponding to the failure of graphene at different temperatures and loading régimes (figure 3) are mapped to the normalized γ^{zz}–γ^{ac} domain and shown in figure 5. Inspection of the results shown indicates that the entire ensemble of data points can be approximated with a bilinear curve reasonably well. The bilinear curve has two distinct segments on both sides of the 1 : 1 line in figure 5. A best-fit curve was obtained using a least squares method in the form of:

$$\gamma_{max} + 0.2\gamma_{min} = 1, \tag{7}$$

which defines a simple bilinear failure envelope for graphene where $\gamma_{max} = \max\{\gamma^{zz}, \gamma^{ac}\}$ and $\gamma_{min} = \min\{\gamma^{zz}, \gamma^{ac}\}$. Equation (7) is a Bayesian change-point model that can capture the abrupt variation in the sequence of the data shown in figure 5 at a change-point of $\gamma^{zz} = \gamma^{ac} = 0.83$ [44]. The non-smooth behavior evinced by equation (7) is similar to that of the maximum shear stress criterion for yield (Tresca) and could be due to an interplay between ductile flow and brittle fracture modes of failure [20]. Since the strain rate was kept the same for all of the simulations that were used to develop equation (7), it is assumed that the failure envelop holds its shape for other strain rates. However, the uniaxial ultimate strength values corresponding to a particular strain rate (see figure 1) must be used to calculate actual applied stresses leading to failure in graphene.

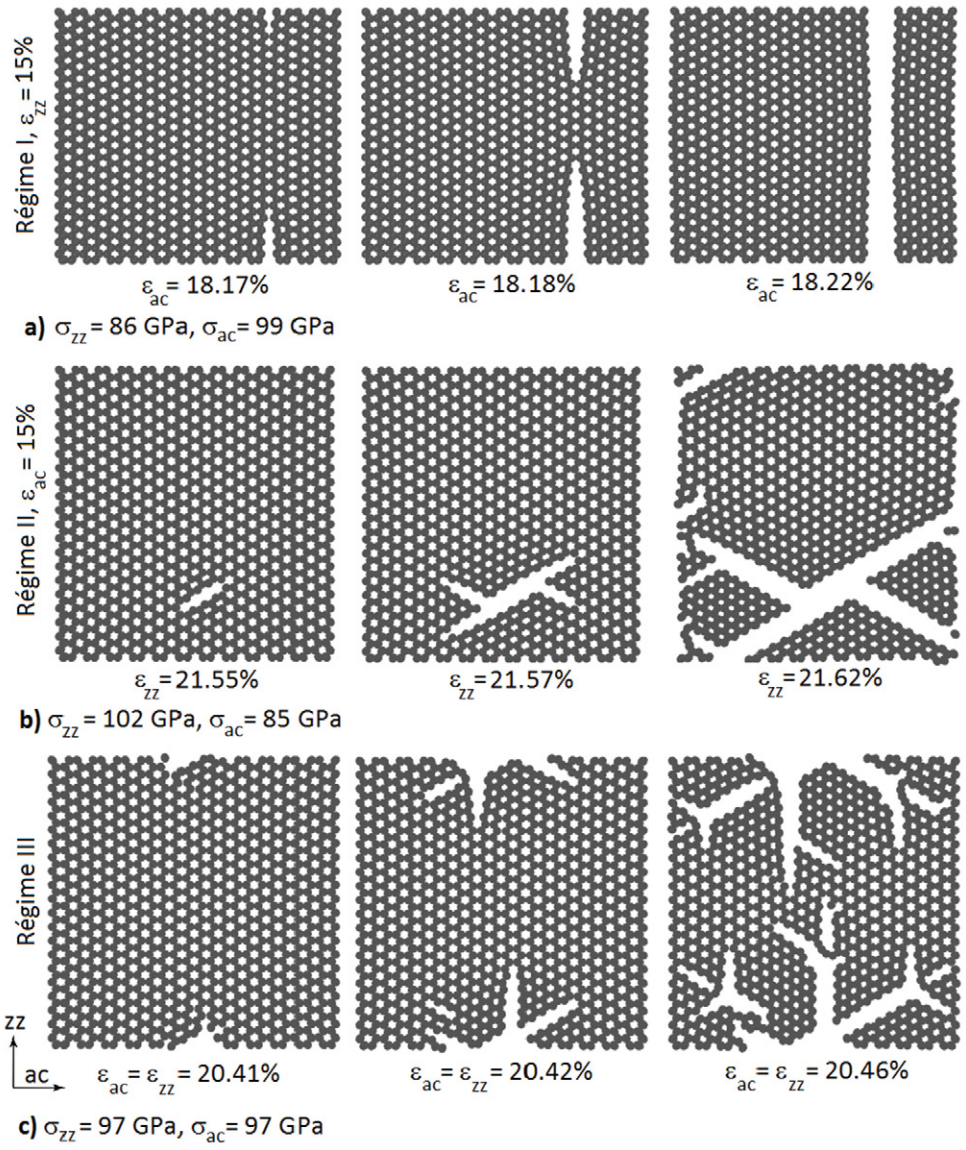

Figure 4. Failure modes of graphene at 0 K under loading régimes (a) I, (b) II and (c) III.

The data and the best-fit bilinear curve shown in the γ^{zz}–γ^{ac} plot of figure 5 represent the critical combinations of γ^{zz} and γ^{ac} which would lead to failure in the graphene sheet. Therefore, the best fit bilinear curve shown in figure 5 is, by definition, a failure envelope for the graphene sheet in biaxial loading.

A second 'unit-circle' failure envelope was also obtained for the data shown in figure 5 analogous to the plasticity models for the prediction of failure in biaxially loaded metal plates [45]. The 'unit-circle' failure envelope defined as:

$$(\gamma^{zz})^2 + (\gamma^{ac})^2 = 1 \tag{8}$$

Table 1. Strain-rate dependent failure properties of graphene under equi-biaxial loading (régime III)

	Strain Rate (0.001 ps^{-1})								
	0.01			1			100		
Temp. (K)	ε_u (%)	$\Delta\sigma^{ac}$ (GPa)	$\Delta\sigma^{zz}$ (GPa)	ε_u (%)	$\Delta\sigma^{ac}$ (GPa)	$\Delta\sigma^{zz}$ (GPa)	ε_u (%)	$\Delta\sigma^{ac}$ (GPa)	$\Delta\sigma^{zz}$ (GPa)
1	20.2	97.5	97.5	20.0	97.3	97.3	22.0	95.2	97.4
300	12.5	79.7	79.8	13.5	82.5	82.8	15.5	86.4	86.6
500	10.1	70.2	70.6	11.0	73.6	73.8	13.5	80.8	81.1
1000	7.6	57.3	56.8	8.0	58.9	58.4	11.0	70.0	67.0
1500	6.6	51.3	49.8	7.0	52.3	51.1	10.5	64.5	64.4

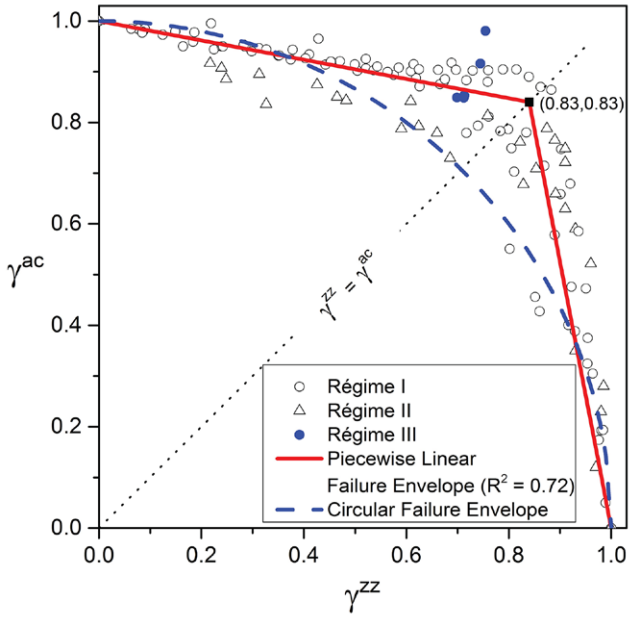

Figure 5. Biaxial failure envelopes for graphene subjected to different loading régimes

provides an appealing, mathematically convenient approximation for the bilinear failure envelope that can be used for the back-of-the-envelope calculation of the graphene ultimate strength in biaxial loading. However, as can be observed in figure 5, the 'unit-circle' failure envelope is less accurate than the bilinear envelope in capturing the predicted ultimate strength data shown in the figure.

4. Conclusions

MD simulations were carried out in order to develop failure criteria for defect-free, infinite graphene tested in biaxial loading at different temperatures. In the MD simulations, a model of graphene sheet was biaxially loaded to failure using different sequences of loading in its zigzag and armchair principal directions. The predicted biaxial failure stresses in the two

principal directions were plotted normalized to their receptive uniaxial ultimate strength values. Bilinear and circular failure envelopes were introduced using a least squares method for practical applications. Results showed that the biaxial failure envelopes for graphene in terms of actual applied stresses are consistently smaller (indicating reduced strength) at elevated temperatures. However, failure envelopes in terms of normalized stresses were found to be essentially temperature independent.

The failure criterion proposed in this study is merely valid for defect-free graphene. However, the structural defects arising during growth or processing of graphene severely deteriorate its mechanical properties. In addition, the potential used in this study (i.e. AIREBO) fails to consider bond-reformation. Similar studies on defective graphene using conservative potentials (e.g. SED-REBO and SED-REBO-S [46]) are encouraged in order to develop comprehensive and more accurate failure criteria.

Acknowledgments

Computational resources for the MD simulations in this study were provided by the OU Supercomputing Center for Education & Research (OSCER). Valuable input and comments by Dr Donald Ward at the Sandia National Laboratories, Dr Wayne Stewart, Dr Takumi Hawa and Nathan Cannon at the University of Oklahoma and Nuwan Dewapriya at Simon Fraser University are gratefully acknowledged.

References

[1] Allen M J, Tung V C and Kaner R B 2010 Honeycomb carbon: a review of graphene *Chem. Rev.* **110** 132–45
[2] Novoselov K S, Geim A K, Morozov S V, Jiang D, Zhang Y, Dubonos S V, Grigorieva I V and Firsov A A 2004 Electric field effect in atomically thin carbon films *Science* **306** 666–9
[3] Fernández-Rossier J, Palacios J J and Brey L 2007 Electronic structure of gated graphene and graphene ribbons *Phys. Rev.* B **75** 205441
[4] Mak K F, Sfeir M Y, Wu Y, Lui C H, Misewich J A and Heinz T F 2008 Measurement of the optical conductivity of graphene *Phys. Rev. Lett.* **101** 196405
[5] Zhang H, Zhou T, Xie G, Cao J and Yang Z 2014 Thermal transport in folded zigzag and armchair graphene nanoribbons *Appl. Phys. Lett.* **104** 241908
[6] Geim A K 2009 Graphene: status and prospects *Science* **324** 1530–4
[7] Koratkar N A 2013 *Graphene in Composite Materials: Synthesis, Characterization and Applications* (Lancaster, PA: DEStech Publications, Inc)
[8] Levy N, Burke S A, Meaker K L, Panlasigui M, Zettl A, Guinea F, Neto A H C and Crommie M F 2010 Strain-induced pseudo–magnetic fields greater than 300 T in graphene nanobubbles *Science* **329** 544–7
[9] Yazdani H, Hatami K, Khosravi E, Harper K and Grady B P 2014 Strain-sensitive conductivity of carbon black-filled PVC composites subjected to cyclic loading *Carbon* **79** 393–405
[10] Konstantinova E, Dantas S O and Barone P M V B 2006 Electronic and elastic properties of 2D carbon planes *Phys. Rev.* B **74** 035417
[11] Liu F, Ming P and Li J 2007 *Ab initio* calculation of ideal strength and phonon instability of graphene under tension *Phys. Rev.* B **76** 064120
[12] Lee C, Wei X, Kysar J W and Hone J 2008 Measurement of the elastic properties and intrinsic strength of monolayer graphene *Science* **321** 385–8
[13] Zhao H, Min K and Aluru N R 2009 Size and chirality dependent elastic properties of graphene nanoribbons under uniaxial tension *Nano Lett.* **9** 3012–5
[14] Lu Q, Gao W and Huang R 2011 Atomistic simulation and continuum modeling of graphene nanoribbons under uniaxial tension *Modelling Simul. Mater. Sci. Eng.* **19** 054006

[15] Zhao H and Aluru N R 2010 Temperature and strain-rate dependent fracture strength of graphene *J. Appl. Phys.* **108** 064321
[16] Dewapriya M A. N, Phani A S and Rajapakse R K N D 2013 Influence of temperature and free edges on the mechanical properties of graphene *Model. Simul. Mater. Sci. Eng.* **21** 065017
[17] Marianetti C and Yevick H 2010 Failure mechanisms of graphene under tension *Phys. Rev. Lett.* **105** 245502
[18] Volokh K Y 2012 On the strength of graphene *J. Appl. Mech.* **79** 064501
[19] Tuleubekov K, Volokh K Y, Stolarski H and Mogilevskaya S G 2013 Strength of graphene in biaxial tension *Eur. J. Mech.* A **39** 291–7
[20] Christensen R M 2013 *The Theory of Materials Failure* (Oxford: Oxford University Press)
[21] Plimpton S 1995 Fast parallel algorithms for short-range molecular dynamics *J. Comput. Phys.* **117** 1–19
[22] Brenner D W 1990 Empirical potential for hydrocarbons for use in simulating the chemical vapor deposition of diamond films *Phys. Rev.* B **42** 9458–71
[23] Pei Q X, Zhang Y W and Shenoy V B 2010 A molecular dynamics study of the mechanical properties of hydrogen functionalized graphene *Carbon* **48** 898–904
[24] Shenderova O A, Brenner D W, Omeltchenko A, Su X and Yang L H 2000 Atomistic modeling of the fracture of polycrystalline diamond *Phys. Rev.* B **61** 3877
[25] Mattoni A, Ippolito M and Colombo L 2007 Atomistic modeling of brittleness in covalent materials *Phys. Rev.* B **76** 224103
[26] Costescu B I, Baldus I B and Gräter F 2014 Graphene mechanics: I. Efficient first principles based Morse potential *Phys. Chem. Chem. Phys.* **16** 12591–8
[27] Xu L, Wei N and Zheng Y 2013 Mechanical properties of highly defective graphene: from brittle rupture to ductile fracture *Nanotechnology* **24** 505703
[28] Tsai D H 1979 The virial theorem and stress calculation in molecular dynamics *J. Chem. Phys.* **70** 1375–82
[29] Subramaniyan A K and Sun C T 2008 Continuum interpretation of virial stress in molecular simulations *Int. J. Solids Struct.* **45** 4340–6
[30] Zhou M 2003 A new look at the atomic level virial stress: on continuum-molecular system equivalence *Proc. R. Soc. Lond. Math. Phys. Eng. Sci.* **459** 2347–92
[31] Andia P C, Costanzo F and Gray G L 2006 A classical mechanics approach to the determination of the stress–strain response of particle systems *Model. Simul. Mater. Sci. Eng.* **14** 741
[32] Yazdani H, Hatami K, Hawa T and Grady B P 2013 Atomic-scale simulation of sensor-enabled geosynthetics for health monitoring of reinforced soil slopes and embankments *Geo-Congress Stability and Performance of Slopes and Embankments III* (San Diego, US: ASCE) pp 1529–35
[33] Dewapriya M A N, Rajapakse R K N D and Phani A S 2014 Atomistic and continuum modelling of temperature-dependent fracture of graphene *Int. J. Fract.* **187** 199–212
[34] Hossain D, Tschopp M A, Ward D K, Bouvard J L, Wang P and Horstemeyer M F 2010 Molecular dynamics simulations of deformation mechanisms of amorphous polyethylene *Polymer* **51** 6071–83
[35] Eftekhari M, Mohammadi S and Khoei A R 2013 Effect of defects on the local shell buckling and post-buckling behavior of single and multi-walled carbon nanotubes *Comput. Mater. Sci.* **79** 736–44
[36] Zandiatashbar A, Lee G-H, An S J, Lee S, Mathew N, Terrones M, Hayashi T, Picu C R, Hone J and Koratkar N 2014 Effect of defects on the intrinsic strength and stiffness of graphene *Nat. Commun.* **5** 3186
[37] Bu H, Chen Y, Zou M, Yi H, Bi K and Ni Z 2009 Atomistic simulations of mechanical properties of graphene nanoribbons *Phys. Lett.* A **373** 3359–62
[38] Dewapriya M A N and Rajapakse R K N D 2014 Molecular dynamics simulations and continuum modeling of temperature and strain rate dependent fracture strength of graphene with vacancy defects *J. Appl. Mech.* **81** 081010
[39] Zhang B, Mei L and Xiao H 2012 Nanofracture in graphene under complex mechanical stresses *Appl. Phys. Lett.* **101** 121915
[40] Whittaker A G 1978 The controversial carbon solid–liquid–vapour triple point *Nature* **276** 695–6
[41] Terdalkar S S, Huang S, Yuan H, Rencis J J, Zhu T and Zhang S 2010 Nanoscale fracture in graphene *Chem. Phys. Lett.* **494** 218–22

[42] Jin C, Lan H, Peng L, Suenaga K and Iijima S 2009 Deriving carbon atomic chains from graphene *Phys. Rev. Lett.* **102** 205501
[43] Topsakal M and Ciraci S 2010 Elastic and plastic deformation of graphene, silicene, and boron nitride honeycomb nanoribbons under uniaxial tension: a first-principles density-functional theory study *Phys. Rev.* B **81** 024107
[44] Barry D and Hartigan J A 1993 A Bayesian analysis for change point problems *J. Am. Stat. Assoc.* **88** 309–19
[45] Kee Paik J 2008 Ultimate strength of perforated steel plates under combined biaxial compression and edge shear loads *Thin-Walled Struct.* **46** 207–13
[46] Perriot R, Gu X, Lin Y, Zhakhovsky V V and Oleynik I I 2013 Screened environment-dependent reactive empirical bond-order potential for atomistic simulations of carbon materials *Phys. Rev.* B **88** 064101